Hindawi
Shock and Vibration
Volume 2019, Article ID 4919505, 13 pages
https://doi.org/10.1155/2019/4919505

Research Article

Multi-DOF Ultrasonic Actuators for Laser Beam Positioning

Ramutis Bansevicius,[1] **Dalius Mazeika**,[2] **Vytautas Jurenas**,[1] **Genadijus Kulvietis**,[2] **and Asta Drukteiniene**[2]

[1]*Kaunas University of Technology, Studentų g. 56, Kaunas LT-51424, Lithuania*
[2]*Vilnius Gediminas Technical University, Saulėtekio al. 11, Vilnius LT-10223, Lithuania*

Correspondence should be addressed to Dalius Mazeika; dalius.mazeika@vgtu.lt

Received 2 October 2018; Revised 7 December 2018; Accepted 22 January 2019; Published 10 February 2019

Academic Editor: Jörg Wallaschek

A novel design concept of multi-degree-of-freedom (multi-DOF) piezoelectric actuator is introduced in the paper. The main idea is to connect two identical piezoelectric transducers by hyperelastic material in order to increase the total number of degrees-of-freedom of the system. Such design principle also allows to separate vibrations of two piezoelectric transducers and to control them independently. The ring- and cylinder-type piezoelectric transducers were used to design two multi-DOF ultrasonic actuators for precise laser beam positioning. Reflecting mirror is mounted on the top of the actuator and is preloaded by magnetic force. Both disc- and cylinder-type actuators can realize up to six degrees-of-freedom, i.e., to rotate the mirror about three axes employing one transducer and to position mirror in the plane by using another transducer. Bidirectional rotation and translation motion of the mirror are obtained by switching excitation signals between different electrodes of the transducers. Both the numerical simulation and physical prototype were used to verify operating principle of the actuators. Numerical investigation of the piezoelectric actuator was performed to investigate modal-frequency and harmonic response analysis while experimental study was performed to measure electrical and mechanical output characteristics of the piezoelectric actuator. A mathematical model of contacting force control was proposed, and numerical verification was performed when the mirror need to be rotated according to the specific motion trajectory.

1. Introduction

Laser optical subsystems are used for different applications such as measurement device, industrial machining tools, and robotics [1]. Ability to adjust the laser beam pointing is crucial for the optical system [2]. Beam needs to be moved in particular position and angle; therefore, different optical-mechanical elements including mirrors, actuators, and controllers are used to project the beam to a target location on the surface. Micrometer scale resolution is required for the most applications; however, the higher resolution allows achieving the higher precision of the measurement device or machining tool [3].

Resolution of the laser beam steering strongly depends on the characteristics of the actuator. Most of the industrial laser optical systems use different types of electrical motors to rotate or move mirrors; however, resolution of such systems is limited to several micrometers. Moreover, conventional single-DOF actuators such as electrical motors require multiple number of actuators to generate a multi-DOF motion [3]. It is difficult to eliminate assembly errors in combining single-DOF actuators, and constant maintenance for eliminating secular error is necessary [4]. Moreover, the mechanical system itself gets more complex. Also, such approach of multi-DOF actuation is not suitable for applications where the weight, size, and high resolution become an issue.

Piezoelectric actuators are capable of reaching nanometric resolution and possess features such as short response time, large output power, compact size, self-braking, and good controllability [5, 6]. Usually, the piezoelectric actuator is a single degree-of-freedom (DOF) device; however, there are several recently developed multi-DOF systems [5]. A multi-DOF piezoelectric ultrasonic

actuator can generate multi-DOF rotation or translation of the positioning system by utilizing natural vibration modes of a stator; therefore, a steering multi-DOF laser beam system can be developed.

A 3-DOF Langevin-type piezoelectric actuator was developed by Zhao [7]. It is composed of a cylindrical stator and a spherical rotor. Actuator operates employing superposition of bending and longitudinal vibration modes when the excitation voltages with certain frequency, phase, and amplitude are applied to the three groups of piezoelectric ceramic rings. A similar ultrasonic motor capable of generating a multi-DOF rotation of a spherical rotor utilizing bending and longitudinal natural vibration modes of a bar-shaped stator was proposed by Tukemura et al. [8]. The multi-DOF master-slave system for laparoscopic surgical procedures was made using this ultrasonic actuator. The 3-DOF piezoelectric actuator generating rotation of the sphere about three axes was developed by Vasiljev et al. [9]. The operation of the actuator is based on a shaking beam principle. The proposed actuator consists of a vibrating beam type frame, four piezoceramic stacks, and four overlays. Four driving tips are mounted on the top of the vibrating frame and are in contact with the sphere. Four electric signals with shifted phases by $\pi/2$ are used for excitation. Gouda et al. proposed multi-DOF small size cylinder type piezoelectric actuator [10]. The actuator consists of a small cylinder fixed on a substrate and a thin piezoceramic ring that is glued to the substrate. The electrodes of piezoceramic ring are divided into four parts and are driven by shifted phase signals. Superposition of the first longitudinal and the second bending mode is used to obtain elliptical vibrations on the top surface of the cylinder as well as rotating a ball about three axes independently. Multi-DOF ultrasonic actuator was developed by Amano et al. [11]. Three sets of piezoelectric elements are installed in the stator, and two bending vibrations perpendicular to each other as well as a longitudinal vibration can be excited independently with three separate electrical ports. A spherical rotor rotates along three perpendicular axes by the combination of these vibrations.

A novel design concept of a multi-DOF piezoelectric actuator is introduced. The ring- and cylinder-type piezoelectric transducers are used to design two multi-DOF ultrasonic actuators for precise laser beam positioning applying the proposed design principle. Both ring- and cylinder-type actuators can realize up to six degrees-of-freedom, i.e., to rotate the mirror about three axes using the first transducer and to position mirror in the plane employing the second transducer. Numerical simulation and experimental measurements have been performed to verify operating principle and output characteristics of the actuator. The results of numerical and experimental investigations are discussed.

2. Design Concept and Operating Principle

In our previous works, it was already shown that a single disc or cylinder type piezoelectric transducer can successfully generate 2DOF translation motion in the plane or rotate a sphere about three axes [12, 13]. It is possible to increase the number of degrees-of-freedom of the actuator based on a single piezoelectric cylinder; however, it is impossible to excite rotational and translation motion independently. Therefore, we have extended our idea of 3-DOF piezoelectric actuator design by introducing a new multi-DOF actuator with two transducers connected by hyperelastic materials such as synthetic rubber. The introduced mechanical system operates as two masses connected by a spring; therefore, it is possible to isolate vibrations of one transducer and to excite particular vibration mode in another transducer. In such way, independent vibrations of particular transducer can be excited which is needed to rotate or to move reflecting mirror.

The introduced piezoelectric actuator has six degrees-of-freedom, i.e., the actuator can rotate the mirror about three axes and to move or rotate itself in the plane. Two implementations of piezoelectric actuators are proposed. In both cases, the operating principle of the actuator is the same. The first actuator is made using two ring-type transducers while the second actuator is based on two cylinder-type transducers. The principle structures of both actuators with the positioning mirror are shown in Figure 1.

The ring-type piezoelectric actuator consists of a mirror 1 that is glued on a hemisphere made from ferromagnetic material 2, three miniature neodymium magnets 3, disk-type piezoelectric transducers 4 and 6, the thin layer ($\Delta_1 = 0.1, \ldots, 1.0$ mm) of a vibration isolating material 5 such as synthetic rubber and three cylindrical neodymium magnets 7 that are fixed to the underside of piezoelectric transducer 6. Piezoelectric rings are made from PZT-8 piezoceramics and have polarization in the axial direction. Outside diameter, inside diameter, and the thickness of both rings are $25\,\text{mm} \times 10\,\text{mm} \times 4\,\text{mm}$, respectively. All magnets are glued to the surfaces of the upper and lower transducers and are used to generate magnetic force as well as being contact points. The magnets 3 are in contact with the hemisphere and are used to transfer vibration of the upper piezoceramic ring 4 into rotation of the hemisphere. The lower piezoceramic ring 6 is used to actuate translation or rotation of the whole actuator itself in the plane by employing magnets 7 that are contacting with the surface 8 of the housing. Magnetic force is employed to preload mirror together with the hemisphere to the upper piezoceramic ring. The lower ring is preloaded to the surface 8 by magnetic force as well. Such clamping mechanism is not rigid type; therefore, mechanical vibrations of the transducer can be transferred into continuous rotation of the mirror or motion of the lower ring on the surface. Electrodes of both piezoelectric rings are divided into three equal sectors as shown in Figure 1(a). Each electrode is excited by separate high frequency harmonic signal $U_1, \ldots, U_6$ (Figure 1(a)).

The hybrid out-of-plane bending and radial vibrations of the piezoelectric rings are excited to obtain elliptical motion of the contacting points and to rotate or move mirror in the plane.

The following electrode excitation schemes of upper transducer 4 are used to rotate the mirror:

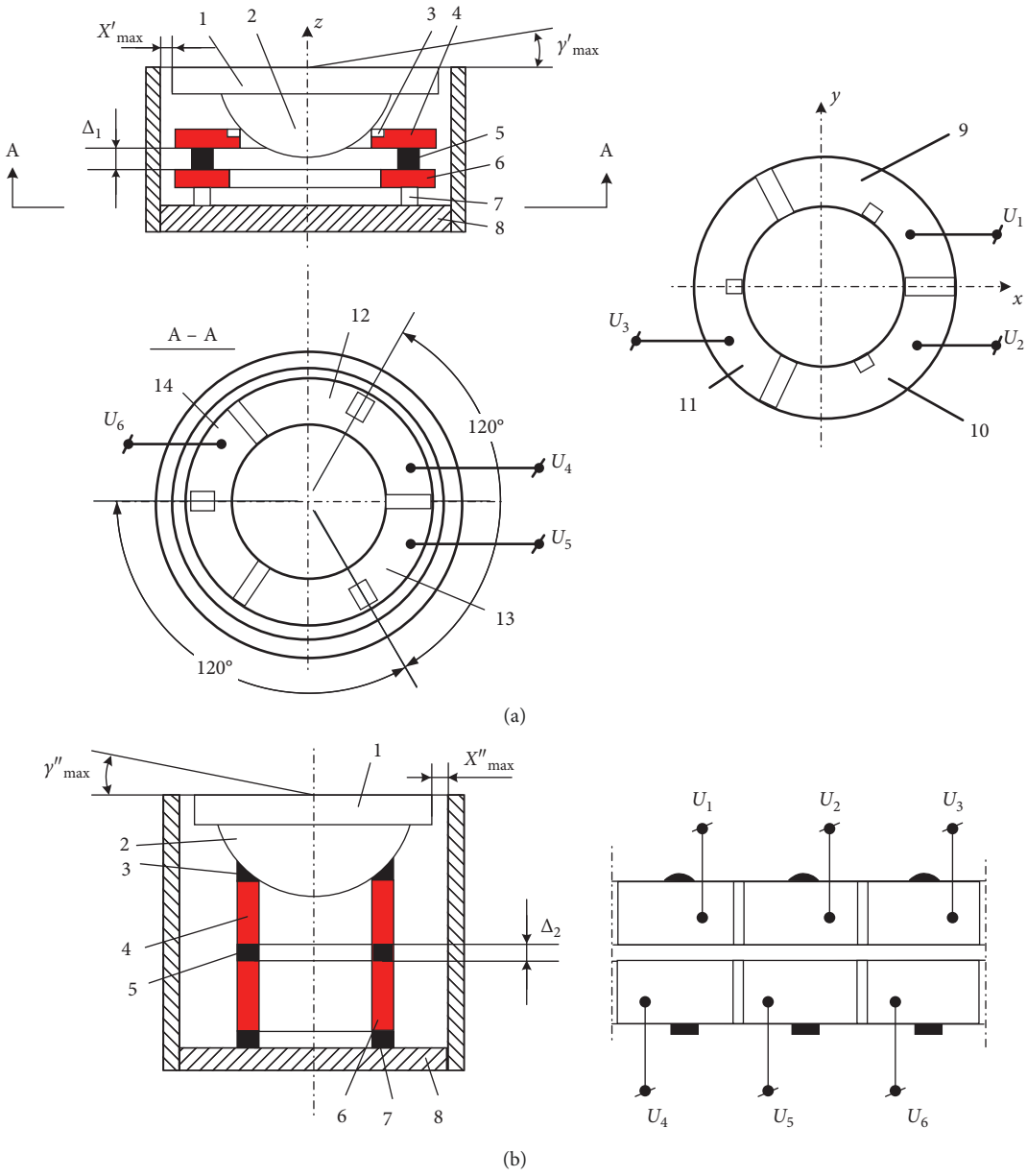

Figure 1: 6-DOF laser beam positioning actuator: ring type (a) and cylinder type (b).

(i) Electrode 11 is excited to obtain rotation of the mirror about y-axis. Reverse rotation is obtained when both electrodes 9 and 10 are excited with the same harmonic signal.

(ii) Rotation about x-axis is obtained when two harmonic signals with different amplitudes and duration is applied to the electrodes 10, 11. Reverse motion is obtained when electrodes 9, 11 are excited. The signal control algorithm used to control excitation of the electrodes is discussed in Section 3.2.

(iii) Rotation of the mirror about z-axis is obtained when electrodes 9, 10, and 11 are excited by three harmonic signals with shifted phase by 120°.

Translation motion of the mirror is obtained when the whole system, i.e., the both transducers and the mirror is moved on the surface 8. The similar electrode excitation schemes of transducer 6 are used to generate translation motion in corresponding directions.

In addition, it must be mentioned that the actuator can be driven by burst type signal in order to achieve very high resolution.

The second 6-DOF actuator has very similar design and is based on two cylinder-type piezoelectric transducers (Figure 1(b)). The numbering of actuator specification is the same as shown in Figure 1(a). Outer diameter, inner diameter, and thickness of the both piezoelectric cylinders are $18 \times 13 \times 13$ mm, respectively. The transducer is made from PZT-8 piezoceramic and has radial polarization. Electrodes of the outer surface of piezoelectric transducer is divided into three equal sections as shown in Figure 1(b). Contacting points are also shown in Figure 1(b). The

electrode of the inner surface is continuous and is grounded. The axial vibration mode of the piezoelectric cylinder is employed to rotate and move the mirror. In summary, it can be noticed that the introduced ring- and cylinder-type multi-DOF actuator can operate in three different modes:

(1) Rotation of the mirror in two directions with high speed but lower resolution

(2) Translation of the mirror in the plane with high speed but lower resolution

(3) Quasistatic rotation of the mirror with high resolution

It also must be pointed that the cylinder-based piezoelectric actuator can achieve large displacement $\gamma''_{\max}$ and $X''_{\max}$, and the resolution can be increased using quasistatic rotation mode of the mirror.

Table 1: Properties of the materials used for simulation.

Material properties	Piezoceramic PZT-8	Neodymium magnet	Silicone
Young's modulus (N/m^2)		$1.6e+11$	$4.2e+6$
Poisson's ratio		0.24	0.43
Density (kg/m^3)	7600	7500	1270
Dielectric permittivity matrix, $x10^{-7}$ (F/m)	$\varepsilon_{11} = 11.42$; $\varepsilon_{33} = 8.85$		
Piezoelectric matrix (C/m^2)	$e_{13} = -18.01$; $e_{33} = 29.48$; $e_{51} = 10.34$		
Elasticity matrix, $x10^{10}$ (N/m^2)	$c_{11} = 14.68$; $c_{12} = 8.108$; $c_{13} = 8.105$; $c_{33} = 13.17$; $c_{44} = 3.29$; $c_{66} = 3.14$		

3. Modeling of the Actuators

Modeling of the proposed piezoelectric actuators consisted of two steps. Firstly, the finite element modeling of the both actuators was performed to confirm and validate operation principle by analyzing motion trajectories of the contact points. Secondly, the mathematical model of contacting force control was developed for hemisphere rotation in particular position.

3.1. Numerical Simulation of the Actuator Vibrations. The numerical study of ring- and cylinder-type actuators consisted of modal-frequency analysis and harmonic response analysis. Trajectories of contact points located on the upper and lower transducers were calculated. FEM software Comsol Multiphysics 5.3a was used to build three-dimensional finite element models of the actuators and to run simulation. Models contained piezoelectric transducers, magnets, and a hyperelastic layer. The mirror and hemisphere were not included into the model. The PZT-8 material was used for modeling piezoceramic rings and cylinders, and solid neodymium properties were applied for cylindrical magnets. The hyperelastic layer was modeled as three rectangular silicone prisms with the dimensions $5 \times 1.5 \times 1.5$ mm. The cylindrical magnets had the following dimensions: Ø2 mm × 1 mm. Properties of the materials are given in Table 1. Both actuators were modeled as not clamped structure. Damping was evaluated in the model by introducing the mechanical loss factor for the piezoceramic transducer. The mechanical loss factor was set to 0.004. Piezoelectric and dielectric losses were neglected in the model. The Mooney–Rivlin model was used to define silicone properties.

Modal-frequency analysis of the actuators was performed to calculate the natural frequencies when the short-circuit boundary conditions were applied. Analyzing oscillation modes of the upper ring-type transducer, it was determined that combination of several oscillation modes can be used to rotate the sphere, i.e., the first radial mode of the ring (64.08 kHz), B07 out-of-plane bending mode (68.73 kHz) and B03 in-plane bending mode (71.18 kHz). In addition, it must be noted that identical vibration modes has the lower ring but the frequencies values are smaller about 0.3 kHz. While analyzing vibration modes of cylinder type transducer, it was found that the cylinder-type piezoelectric actuator has a mode where radial and bending vibrations are dominating (83.16 kHz). This vibration mode can be used to rotate and move the mirror.

Harmonic response analysis was performed to find out the response of the contact point to the sinusoidal voltage applied to the electrodes and to calculate trajectories of the contact point motion. Vibrations of one contact point located on the top and bottom surfaces were investigated because of the symmetry of the structure. One electrode that is closest to contact point was excited, and contact point trajectory was calculated. A 100 V AC signal was applied to the electrode. A frequency range from 50 kHz until 90 kHz with a solution at 50 Hz intervals were chosen for the ring-type actuator, and adequate response curves of contact point vibration amplitudes were calculated. The frequency range for the cylinder-type actuator was from 78 kHz until 85 kHz, respectively. The results are given in Figures 2 and 3 where the contact point vibration amplitudes versus frequency are shown for the upper and lower transducers of the ring- and cylinder-type actuators. All graphs show amplitude projections in x, y, and z axes. Modes of vibrations that were chosen as operating modes of the actuators are shown as in Figures 4 and 5. Total displacements are represented in different colors in these figures.

Analyzing results of simulation, it can be noticed that contact point vibrates in the xz plane. Also, several peaks can be seen in the graphs that correspond to different vibration modes of the actuator. The operating mode of the ring-type actuator is excited when the harmonic signal of the frequency 67.05 kHz is applied to the upper ring and 65.80 kHz signal is applied to the lower ring. The difference between resonant frequencies is 1.25 kHz. It mainly comes because of the different dimensions of the magnets glued to the upper

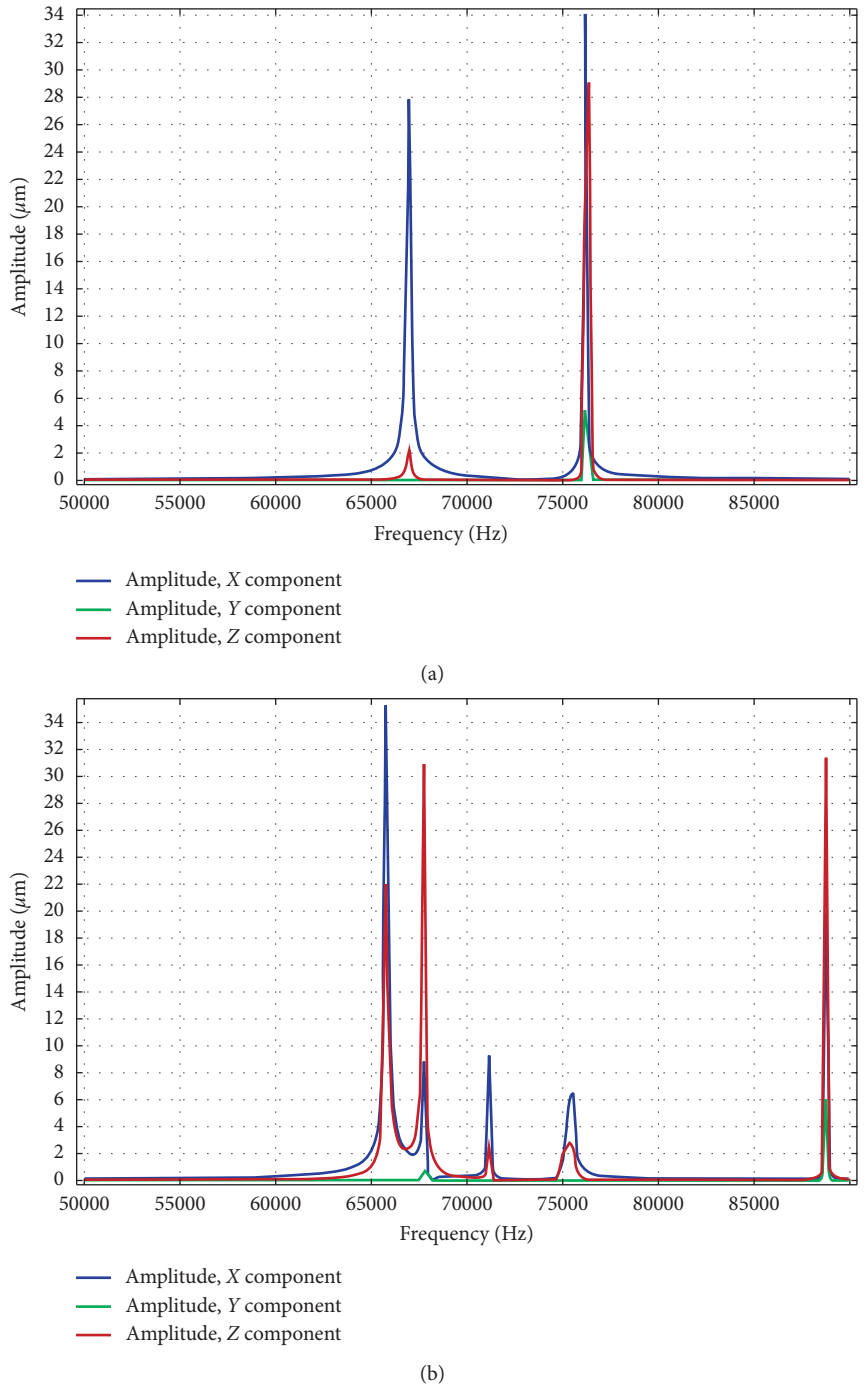

Figure 2: Amplitude-frequency characteristic of the contact points vibrations when the single electrode of the upper ring (a) and lower ring (b) is excited.

and lower rings. In addition, it can be seen that vibration of the contact point are dominating in the x direction. The operating mode of the cylinder-type transducer is excited when the harmonic signal of the resonant frequency 81.55 kHz and 80.90 kHz is applied to upper and lower cylinders, respectively. The difference between resonant frequencies is 0.65 kHz, and the reason of this difference is the same as for the ring-type actuator. Analyzing contact point vibration amplitude values of different actuators, it can be seen that ring-type actuator achieves larger amplitudes of vibration. This can be explained by the fact that the stiffness of the ring transducers is smaller; therefore, vibration amplitudes are higher.

Trajectories of the contact point motion were calculated as well (Figure 6). It can be seen that trajectories have ellipsoidal shapes. Length of the major ellipsis axis is 81.03 μm and 54.5 μm for ring-type transducers and 14.1 μm and 5.49 μm. Numerical simulations confirmed

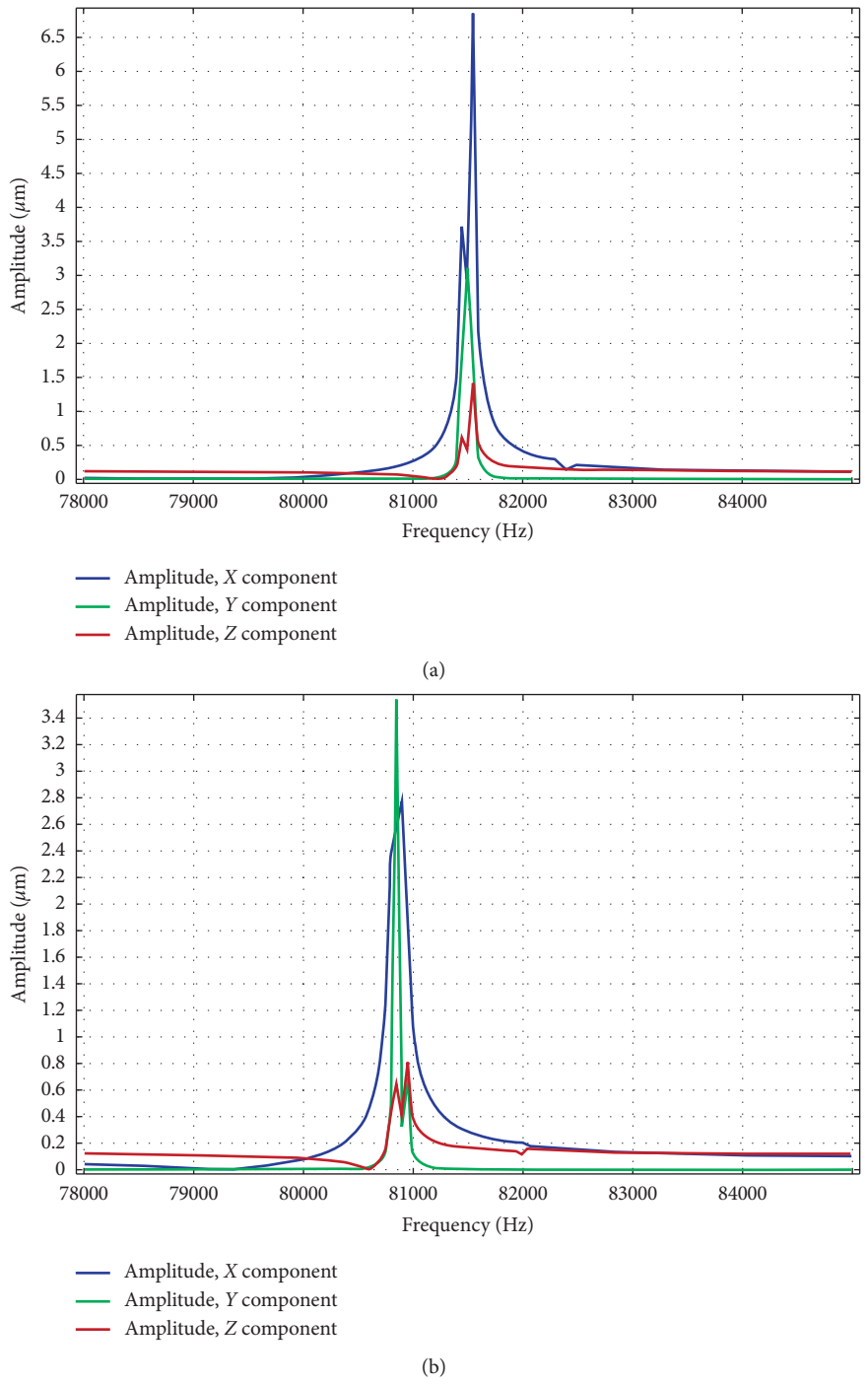

Figure 3: Amplitude-frequency characteristic of the contact points vibrations when the single electrode of the upper cylinder (a) and lower cylinder (b) is excited.

that elliptical trajectories of contact point motion can be excited applying aforementioned excitation schemes and the actuator can rotate and move the laser beam reflecting mirror.

3.2. Mathematical Modeling of Mirror Rotation Control. The aim of this study was to build a mathematical model for the mirror rotation control by maximizing rotation velocity. A sphere was used in the model instead of the mirror and hemisphere. The model was developed for the cylinder-type transducer but it can be used for the disc-type transducer as well. It was assumed in the model that rotation of the sphere is obtained by applying three equivalent contact forces that have predefined directions as it is shown in Figure 7. In addition, it was assumed that all three electrodes can be excited independently, i.e., three-channel generator is used to drive the

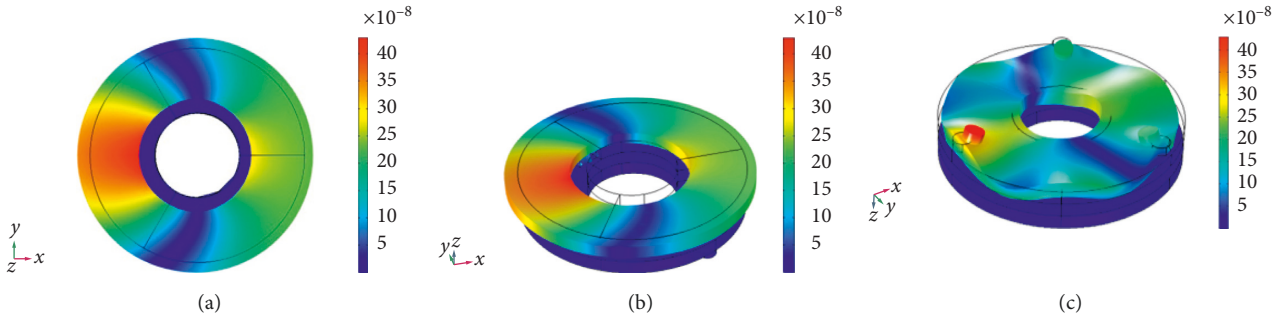

Figure 4: Vibration modes of the ring-type actuator when the upper ring is excited at 67.05 kHz (a, b) and the lower ring is excited at 65.80 kHz (c).

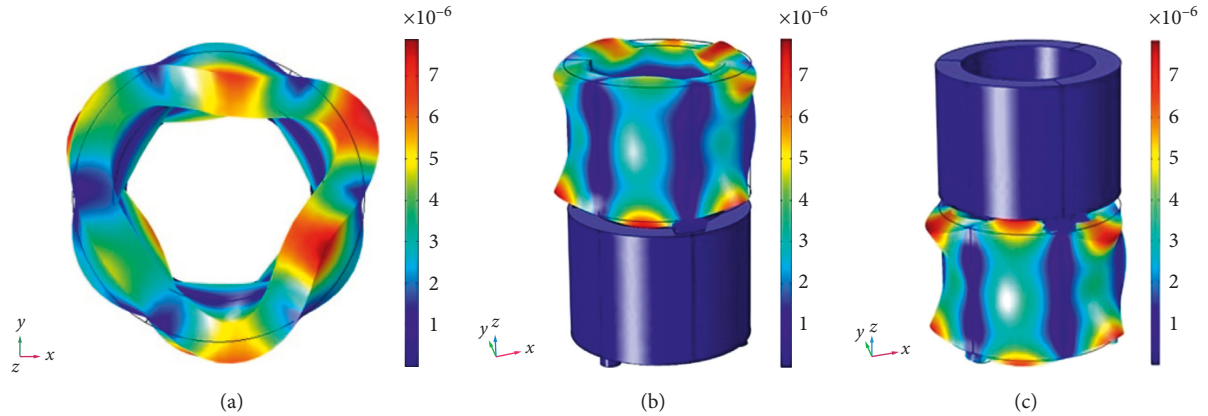

Figure 5: Vibration modes of the cylinder-type actuator when the upper cylinder is excited at 81.55 kHz (a, b) and the lower cylinder is excited at 80.90 kHz (c).

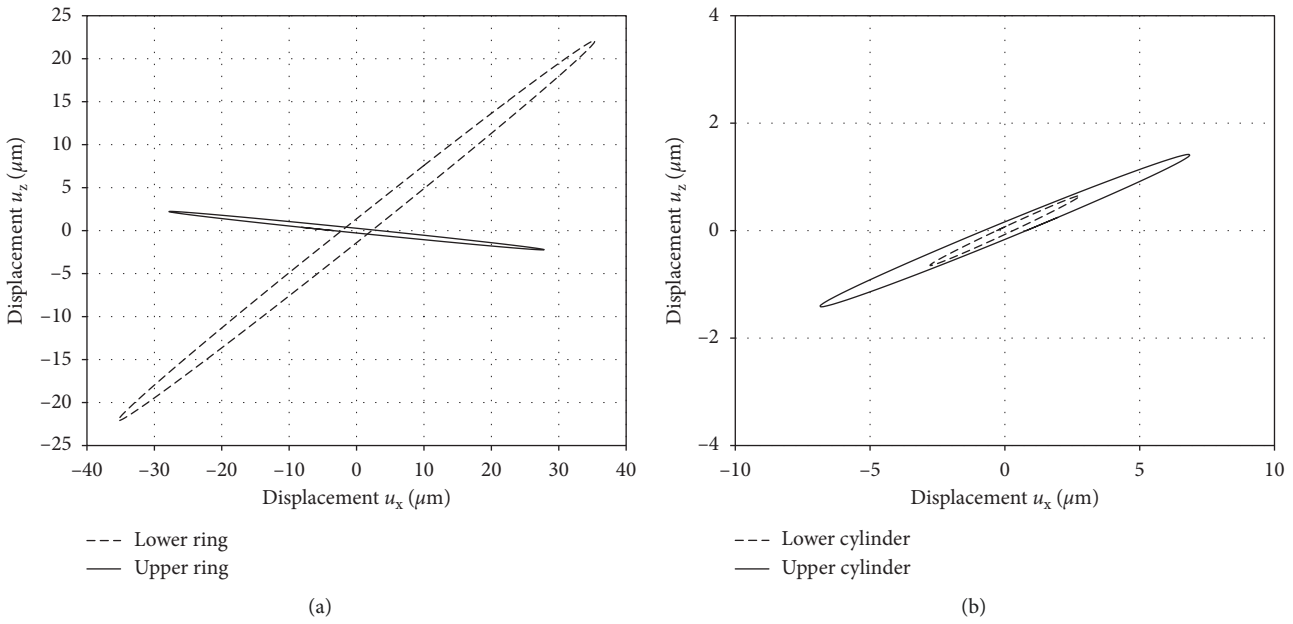

Figure 6: Contact point vibration trajectories of the ring-type actuator (a) and cylinder-type actuator (b).

transducer. When electric signals are applied to the electrode, equivalent contact force vector is generated with specific values $\vec{C}_J(t)$ and the resultant equivalent force can be calculated. Here, J is a number of contacting point, where $J = 1, 2, 3$ and t is a time parameter of the equivalent force function.

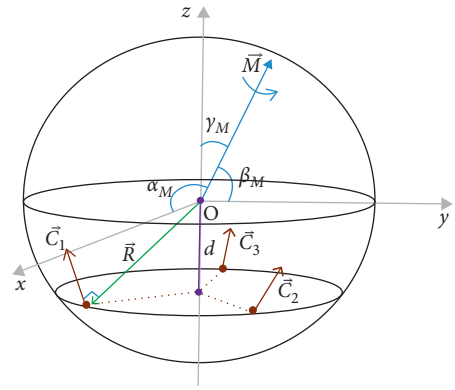

Figure 7: Schematic drawing of the rotating sphere.

Let us assume that orientation of equivalent contact force vector does not change during all rotation time of the sphere:

$$\vec{C}_J = \left(\cos\,\alpha_J,\ \cos\,\beta_J,\ \cos\,\gamma_J\right) = \text{const}, \tag{1}$$

where α_J, β_J, and γ_J are the angles between x, y, and z axes and equivalent forces $\vec{C}_J$. Then, orientations of $\vec{C}_J$ can be calculated by using the following formula [14]:

$$\left[\vec{C}_J\left(\alpha_J, \beta_J, \gamma_J\right)\right] = \cos^{-1}\begin{bmatrix} \dfrac{d}{|\vec{R}|} & 0 & \sqrt{1-\left(\dfrac{d}{|\vec{R}|}\right)^2} \\ -\dfrac{d}{2R} & \dfrac{\sqrt{3}}{2}\dfrac{d}{R} & \sqrt{1-\left(\dfrac{d}{|\vec{R}|}\right)^2} \\ -\dfrac{d}{2R} & \cos\left(180^\circ - \cos^{-1}\left(\dfrac{\sqrt{3}}{2}\dfrac{d}{R}\right)\right) & \sqrt{1-\left(\dfrac{d}{|\vec{R}|}\right)^2} \end{bmatrix}, \tag{2}$$

where $|\vec{R}|$ is radius of the sphere and d is a distance from the center of the sphere till the plane, where contacts of cylinder are located and $d < |\vec{R}|$. Rotation of the sphere can be described as a vector function $\vec{r}\,(|\vec{R}|, \theta(t), \phi(t))$, where $\theta \in [0, \pi]$ is angle between positive z-axis and $\vec{r}$; $\phi(t) \in [0, 2\pi)$ is an angle between positive x-axis and projection in xy plane of vector $\vec{r}$.

In this case, the direction of sphere rotation can be defined. The direction is the same as direction of the unit tangent vector at time point t of the function $\vec{r}\,(t)$. The unit tangent vector also shows direction of the total equivalent force. The unit tangent vector $\vec{T}\,(t) = \langle T_x | T_y | T_z \rangle$ is calculated as follows:

$$\vec{T}\,(t) = \frac{\vec{r}\,'(t)}{\left|\vec{r}\,'(t)\right|} = \frac{1}{\left|\vec{r}\,'(t)\right|}\langle x'(t)\,|\,y'(t)\,|\,z'(t)\rangle, \tag{3}$$

where

$$\vec{r}\,(t) = \begin{cases} x(t) = |\vec{R}|\sin\theta(t)\cos\phi(t), \\ y(t) = |\vec{R}|\sin\theta(t)\sin\phi(t), \\ z(t) = |\vec{R}|\cos\theta(t). \end{cases} \tag{4}$$

The fine trajectory planning algorithm can be used for the problem solving [15]. It requires projections of unit tangent vector $\vec{F}_i$ and component $\vec{f}_J$ in the xy plane. Values of the components projections are calculated by the using the following formula:

$$\frac{\left|\vec{f}_{Ji}\right|}{\cos(90^\circ - \theta)} = \begin{cases} f_{\min}, & \text{if } \varphi_{Ji} \geq \beta, \\ f_{\max}, & \text{if } \varphi_{Ji} = \min\left(\left[\varphi_{Ji}\right]\right), \\ \left|\vec{f}^{\,*}_{Ji}\right|, & \text{else}, \end{cases} \tag{5}$$

where $\varphi_{Ji} = \widehat{\vec{F}_i \vec{f}_{Ji}}$. The force that is the nearest to the projections of the unit tangent vector orientation is equal to maximum value while the other force that has opposite orientation is equal to the minimum value (Figure 8).

The values $|\vec{f}^{*}_{Ji}|$ and $|\vec{F}_i|$ are calculated by solving a system of equations:

$$\begin{cases} \left|\vec{F}_i\right|\cos\mu(t) = \sum_{J=1}^{c}\left|\vec{f}_{Ji}\right|\cos\varphi_{Ji}, \\ \left|\vec{F}_i\right|\sin\mu(t) = \sum_{J=1}^{c}\left|\vec{f}_{Ji}\right|\sin\varphi_{Ji}, \end{cases} \tag{6}$$

where $\mu(t) = \tan^{-1}(T_y(t)/T_x(t))$.

Then, equivalent force obtained in the particular segment is equal to

$$\left|\vec{C}_J(t)\right| = \left|\vec{f}_{Ji}\right|\cos(90^\circ - \theta). \tag{7}$$

The total equivalent force at the time point t can be calculated as follows:

$$\vec{C}(t) = \sum_{J=1}^{c}\vec{C}_J(t). \tag{8}$$

Several numerical experiments were carried out to validate the mathematical model. The following rotation cases of the sphere were simulated and analyzed: rotation about the z and y axes and sphere rotation according to the specific function. Radius of sphere was set to $R = 50$ mm, and distance from center of the sphere till the contacting point was set to $d = 30$ mm.

The first experiment was performed to simulate rotation of the sphere about the z-axis. The rotation was described as the following function when $\theta(t) = \text{const}$:

$$\vec{r}(t) = \begin{cases} \phi(t) = 90t, \\ \theta(t) = [30^\circ, 90^\circ], \end{cases} \quad \text{where } t \in [0, 2]. \tag{9}$$

Analysis of the results showed that calculated values of the equivalent contacting forces were the same at the different angle $\theta(t)$ (Figure 9).

The next numerical experiment was carried out to calculate rotation of the sphere around the y-axis. In this case, rotation was described as the following function where $\phi(t) = \text{const}$:

$$\vec{r}(t) = \begin{cases} \phi(t) = [0^\circ, 20^\circ], \\ \theta(t) = 90t, \end{cases} \quad \text{where } t \in [0, 2]. \tag{10}$$

Values of the equivalent contact forces did not change during rotation of the sphere and were independent of angle $\theta(t)$. Results of experiments are showed in Table 2.

In the first case, when $\phi(t) = 0^\circ$, rotation trajectory coincided with the first segment of cylinder. Therefore this segment should have the maximum value of equivalent contact force. The last numerical experiment was made to analyze rotation of the sphere when rotation function is described as the following function:

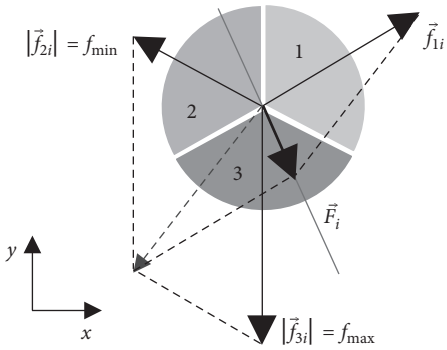

Figure 8: Orientation of the forces in the xy plane.

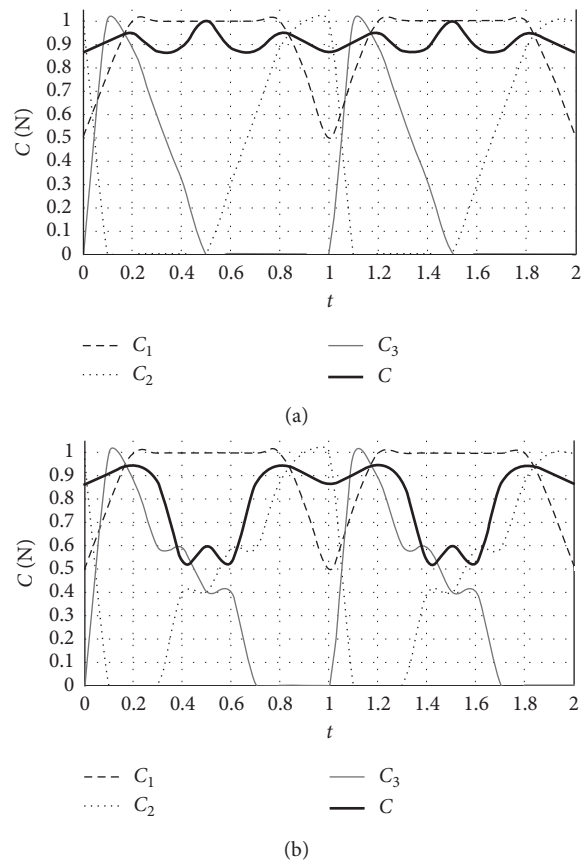

Figure 9: Graph of calculated equivalent contact forces when rotation of the sphere about the z axis is simulated. (a) $C \in [0, 1]$N. (b) $C \in [0.4, 1]$N.

Table 2: Calculated values of the equivalent contact forces.

$[f_{\min}, f_{\max}]$ (N)	$\phi(t)$ (°)	C_1 (N)	C_2 (N)	C_3 (N)	C (N)
[0, 1]	0	1	0	0	1
[0.4, 1]					
[0, 1]	20	1	0.347	0	0.879
[0.4, 1]		1	0.608	0.400	0.528

$$\vec{r}(t) = \begin{cases} \phi(t) = 45t, \\ \theta(t) = 30 + 10t. \end{cases} \quad (11)$$

The results of the experiment are presented in Figure 10. Numerical experiments validated the proposed mathematical model of the equivalent contact force control. Positioning of the sphere is performed at the maximum speed when the fine trajectory planning algorithm and proposed model are used.

4. Experimental Study

A prototype multi-DOF piezoelectric actuators were fabricated for experimental study (Figure 11). The goal of experiment was to validate operating principle of the actuator and to verify results of numerical modeling. Measurements of the prototypes were performed to investigate vibration modes of piezoelectric transducers and identify resonant frequencies. The following equipment was used: 3D scanning vibrometer PSV-500-3D-HV (Polytec GmbH, Germany), linear amplifier P200 (FLC Electronics AB, Sweden) and impedance analyzer 6500B (Wayne Kerr Electronics Ltd., GB). The experimental setup used to measure vibration amplitudes of the upper surfaces of the transducers is shown in Figure 12.

Measurements of electric impedance versus frequency of the both actuators were performed. The analyzed frequency range was 20–150 kHz. Results of measurements are shown in Figures 13 and 14. Two peaks can be seen in Figures 13(a) and 13(b) in frequency range from 60 kHz till 80 kHz. The similar two peaks can be seen in Figure 2(a) where results of numerical simulation of the upper ring is shown. The left peak corresponds to the driving frequency of the upper ring in both graphs. Measured driving frequency of the upper ring is 69.0 kHz. Comparing results of numerical and experimental studies of the lower ring presented in Figures 2(b) and 13(b), it can be noticed that numerical results shows two more resonances at the higher frequencies that were filtered during experimental measurement. However, measured operating frequency of 67.8 kHz has very small error compared to the calculated frequency. The difference between calculated and measured resonant frequencies does not exceed 2.95%. Comparing results of numerical and experimental studies of the cylinder-type actuator, it can be noticed that, in the both cases, a single resonant frequency is obtained in the frequency range 78–85 kHz. Measured driving frequency of the cylinder-type actuator is 82.1 kHz and 79.5 kHz for the upper and lower ring transducer, respectively. The difference between calculated and measured resonant frequencies is not more than 1.7%. The errors mainly came from FEM simulation, such as the inaccuracy of material properties, neglecting glue layer between magnetic cylinder and transducer. The driving voltage of 10 V sinusoidal wave within the scanning frequency range of 20–150 kHz was used to measure vibration amplitudes of the upper surfaces of the transducers using the 3D Polytec vibrometer. The single electrode of the transducer was excited. The result of the measurements is shown in Figure 15. It can be noted that the shape of the measured

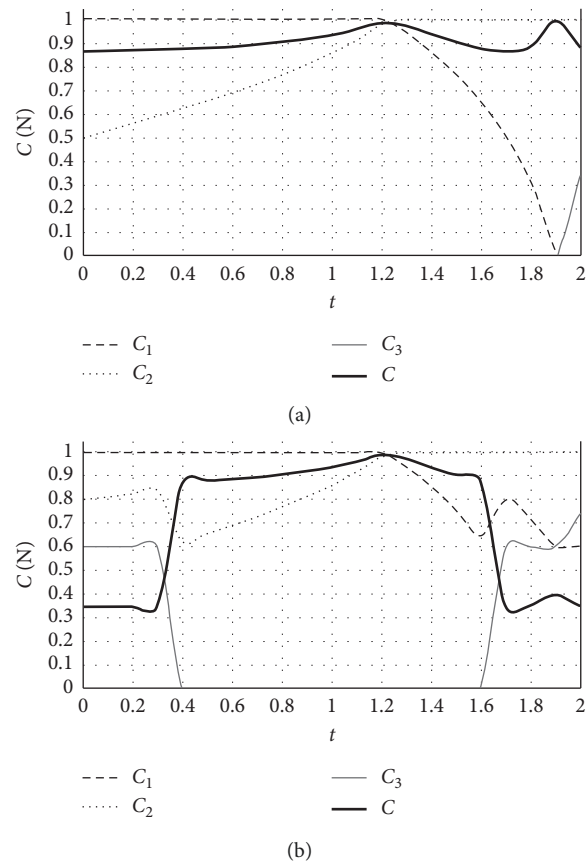

Figure 10: Graph of calculated equivalent contact forces when rotation of the sphere is simulated. (a) $C \in [0, 1]$N. (b) $C \in [0.6, 1]$N.

vibration mode is the similar as it was obtained during numerical simulation (Figures 4(a) and 5(a)).

Resolution of the rotation angle of the mirror and translation resolution were measured using the 3D Polytec vibrometer. Measurements of the cylinder-type actuator were carried out. Upper and lower piezoelectric transducers were driven using burst-type harmonic signal consisting of 20 cycles. Results of the displacement in x direction and rotation angle measurement about y-axis are shown in Figure 16. The minimal resolution of rotation angle is 30 μrad, while rotation speed is 25 μrad/s. In case of translation, the minimal resolution is 0.13 μm and speed is 0.13 μm/s. Also, the both actuators can operate in quasistatic mode when the 200 V electric signal with the frequency of 10 Hz is applied. The experiment study showed that the cylinder-type actuator can achieve angular resolution of 20 μrad while resolution of translation motion can less than 5 μm. The ring-type actuator achieved angular resolution up to 10 μrad, and the resolution of translation motion was less than 1 μm. It must be noted that the resolution of the laser beam positioning depends on the distance between the laser and reflecting mirror, i.e., when the distance is increasing, the resolution is decreasing. The proposed multi-DOF actuators allow achieving micrometer scale resolution of the laser beam positioning when the laser is located at the distance up to 2 meters from the reflecting mirror.

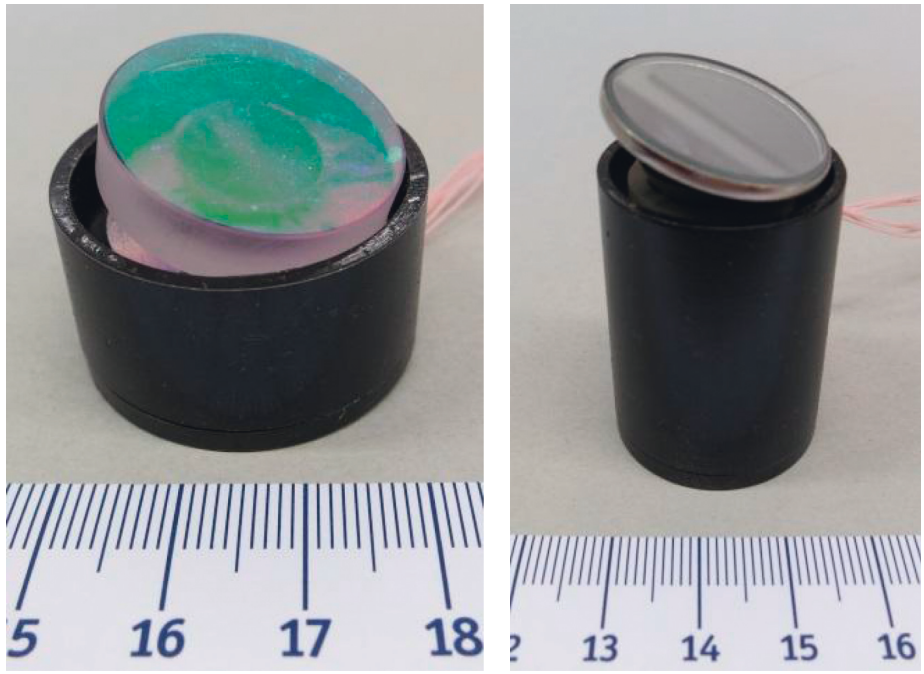

(a) (b)

Figure 11: Prototype multi-DOF piezoelectric actuators with positioning mirror: ring type (a) and cylinder type (b).

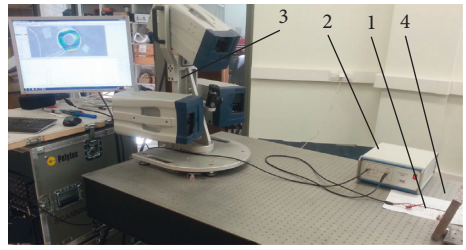

Figure 12: Experimental setup: 1, piezoelectric transducer; 2, liner amplifier P200; 3, 3D scanning vibrometer PSV-500-3D-HV; 4, support of the measured object.

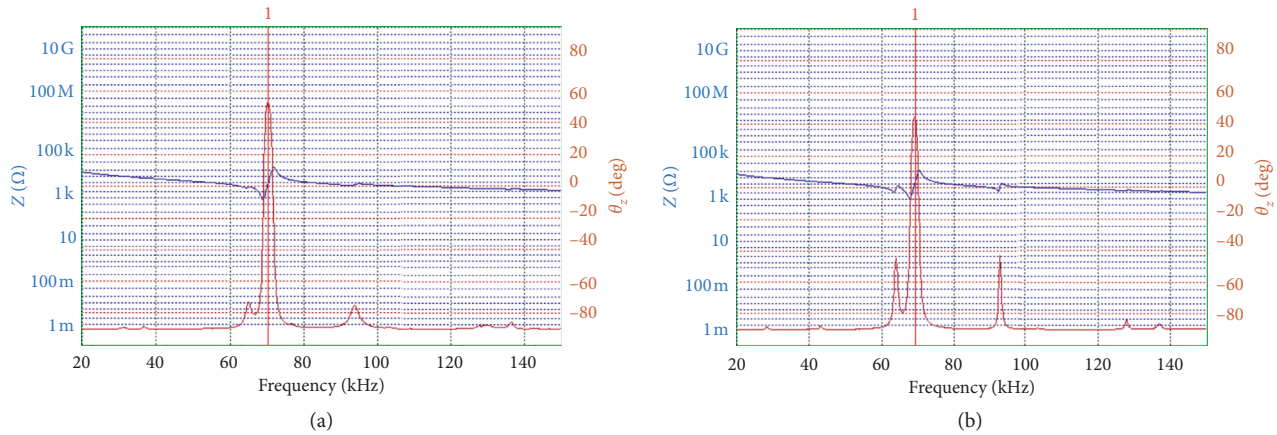

Figure 13: Results of impedance and phase angle spectra measurement of ring-type transducers: measurement of upper transducer, driving frequency is 69.0 kHz (a); measurement of lower transducer, driving frequency is 67.8 kHz (b).

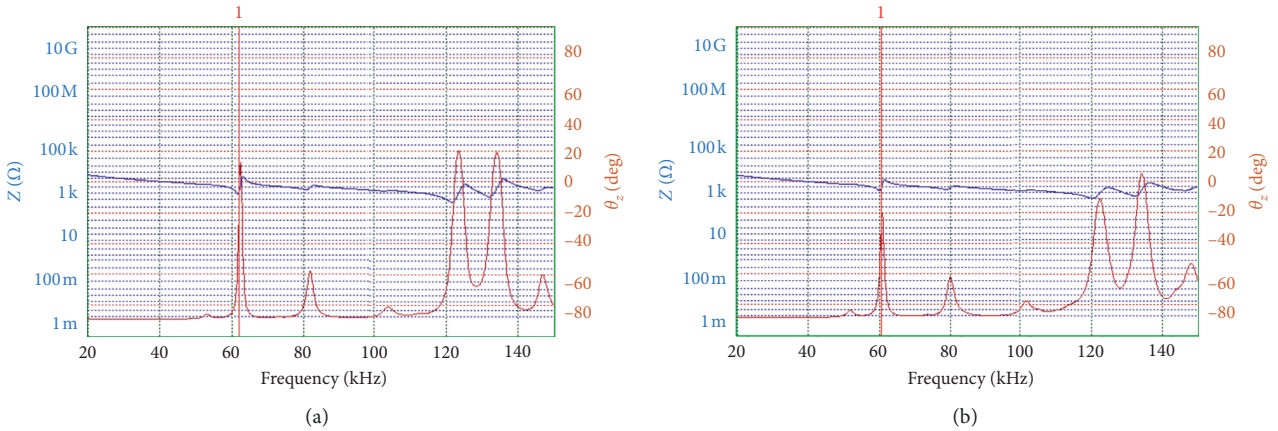

Figure 14: Results of impedance and phase angle spectra measurement of cylinder-type transducers: measurement of upper transducer, driving frequency is 82.1 kHz (a); measurement of lower transducer, driving frequency is 79.5 kHz (b).

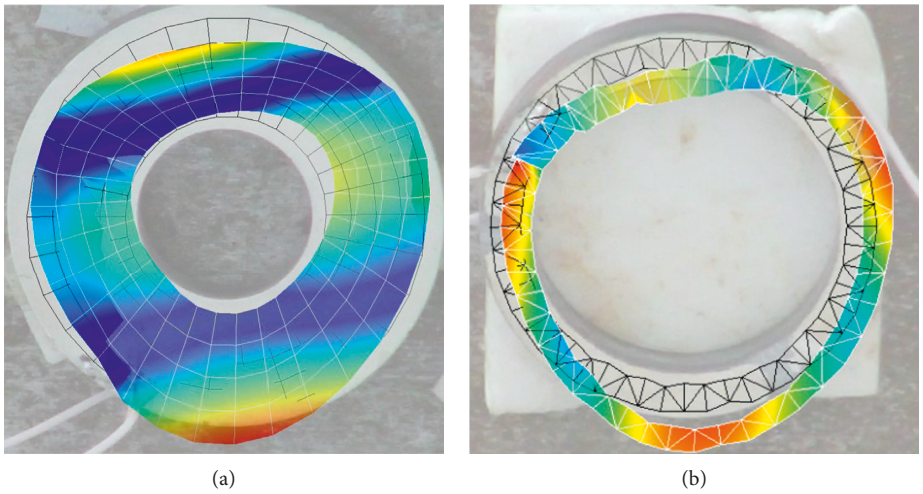

Figure 15: Measured resonance modes of the piezoelectric transducers: ring-type transducer at the frequency of 69 kHz (a), cylindertype transducer at the frequency of 80 kHz (b).

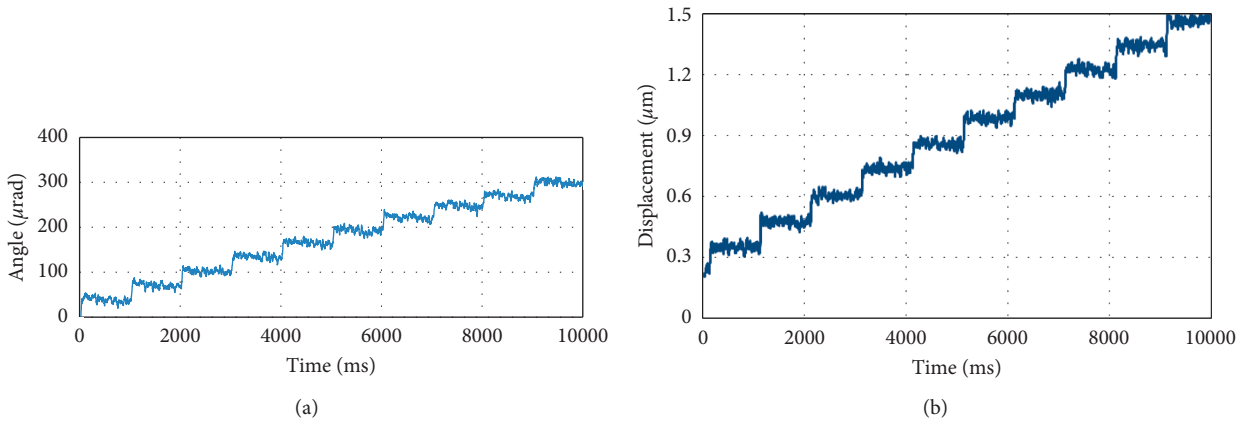

Figure 16: Measured stepped rotation (a) and translation (b) of the mirror using the burst-type harmonic signal.

5. Conclusion

The novel design concept of the multi-DOF piezoelectric actuator was introduced, and two multi-DOF actuators based on ring- and cylinder-type transducers were built. The actuators have a simple design and can achieve microscale resolution of the rotation angle and translation motion. Numerical analysis of piezoelectric actuators has shown the possibilities of achieving elliptical trajectory of the contact point motion. A prototype of multi-DOF piezoelectric actuators was fabricated, and minimal angular resolution of 30 μrad was achieved of cylinder-type actuator. Both actuators can operate in resonant mode and quasistatic mode. Angular resolution of 10 μrad and translation resolution of 1 μm can be obtained when the ring-type actuator operated in the quasistatic mode. The angular and translation resolution of 20 μrad and 5 μm were achieved by using the cylinder-type actuator.

Data Availability

The numerical simulation and experimental measurement data used to support the findings of this study are included within the article. The unprocessed measurement data used to support the findings of this study are available from the corresponding author upon request.

Conflicts of Interest

The authors declare that they have no conflicts of interest.

Acknowledgments

This research was funded by the European Regional Development Fund according to the supported activity No. 01.2.2-LMT-K-718 under the project No. DOTSUT-234.

References

[1] P. Milonni and J. Eberly, *Laser Physics*, Wiley, Hoboken, NJ, USA, 2010.

[2] R.-F. Fung and S.-C. Chao, "Dynamic analysis of an optical beam deflector," *Sensors and Actuators A: Physical*, vol. 84, no. 1-2, pp. 1–6, 2000.

[3] T. Yano, T. Takatsuji, S. Osawa, T. Suzuki, Y. Motomura, and T. Itabe, "Development of a small two Axis spherical motor type laser tracker with submicron measurement accuracy," *IEEJ Transactions on Sensors and Micromachines*, vol. 126, no. 4, pp. 144–149, 2006.

[4] T. Yano, "Actuator with multi degrees of freedom," in *Next-Generation Actuators Leading Breakthroughs*, T. Higuchi, K. Suzumori, and S. Tadokoro, Eds., Springer, London, UK, 2010.

[5] K. Uchino and J. Giniewicz, *Micromechatronics*, Marcel Dekker, New York, NY, USA, 2003.

[6] J. Peng and X. Chen, "A survey of modeling and control of piezoelectric actuators," *Modern Mechanical Engineering*, vol. 3, no. 1, pp. 1–20, 2013.

[7] C. Zhao, *Ultrasonic Motors: Technologies and Application*, Springer, Beijing, China, 2010.

[8] K. Takemura, S. Park, and T. Maeno, "Control of multi-DOF ultrasonic actuator for dexterous surgical instrument," *Journal of Sound and Vibration*, vol. 311, no. 3–5, pp. 652–666, 2008.

[9] P. Vasiljev, D. Mažeika, G. Kulvietis, and S. Vaičiulienė, "Piezoelectric actuator generating 3D-rotations of a sphere," *Solid State Phenomena*, vol. 113, pp. 173–178, 2006.

[10] Y. Gouda, K. Nakamura, and S. Ueha, "A miniaturization of the multi-degree-of-freedom ultrasonic actuator using a small cylinder fixed on a substrate," in *Proceedings of the 2nd International Workshop on Piezoelectric Materials and Applications in Actuators*, pp. 263–267, Paderborn, Germany, 2005.

[11] T. Amano, T. Ishii, K. Nakamura, and S. Uehara, "An ultrasonic actuator with multi-degree of freedom using bending and longitudinal vibrations of a single stator," in *Proceedings of the IEEE International Ultrasonics Symposium*, pp. 667–670, Glasgow, UK, September 1998.

[12] R. Bansevičius, S. Navickaitė, V. Jūrėnas, V. Mačiukienė, G. Kulvietis, and D. Mažeika, "Piezoelectric laser beam deflector for space applications," *Journal of Vibroengineering*, vol. 18, no. 2, pp. 2240–2247, 2016.

[13] R. Bansevicius, A. Drukteiniene, G. Kulvietis, and D. Mazeika, "Switching leg method for trajectory planning of mobile piezorobot," *Journal of Vibroengineering*, vol. 12, no. 1, pp. 26–33, 2010.

[14] R. Bansevičius, G. Kulvietis, D. Mažeika, A. Drukteinienė, I. Tumasonienė, and V. Bakanauskas, "The synthesis of trajectories in piezoelectric attitude control devices for nanosatellites," *Journal of vibration Engineering & Technologies*, vol. 3, no. 3, pp. 345–353, 2015.

[15] R. Bansevicius, A. Drukteiniene, G. Kulvietis, E. Macerauskas, J. Janutenaite, and D. Mazeika, "Fine trajectory planning method for mobile piezorobots," *Journal of Vibroengineering*, vol. 18, no. 4, pp. 2043–2052, 2016.